Day-ahead Risk-constrained Stochastic Scheduling of Multi-energy System

Yue Yin, Tianqi Liu, Lei Wu, Chuan He, and Yikui Liu

Abstract—As an increasing penetration of renewable energy sources can potentially impact voltage profile and compromise system security, the security continues to be the most critical concern in power system operations. A risk-constrained stochastic scheduling model is proposed to leverage the latent scheduling capacity of a multi-energy system to seek an economic operation solution while maintaining system operation risk level against uncertain renewable generation. Overvoltage risk constraints, as compared to the straightforward voltage boundary limits, are incorporated into the stochastic scheduling model to guarantee the operation security and economics. Linearized AC power flow model is applied to enable overvoltage risk assessment within the coordinated scheduling model. The proposed stochastic scheduling model is tackled via the improved progressive hedging approach with an enhanced relax-round-polish process, which overcomes the convergence issues of the traditional progressive hedging in handling nonconvex stochastic scheduling model with binary variables on both stages. Numerical simulation results of IEEE 30-bus system and IEEE 118-bus system illustrate the efficacy of the proposed model in ensuring voltage security and improving economic operation of systems.

Index Terms—AC power flow, overvoltage risk constraint, renewable energy, multi-energy coordination.

I. INTRODUCTION

IN order to achieve environmental sustainability, renewable energy sources, such as wind, solar, and hydro, are being widely deployed in power systems [1]. However, renewable generation usually needs to be transmitted over long distances to load centers. It is easy to induce an excessive voltage drop along long-distance transmission lines and increase the reactive power losses, which will seriously affect the voltage security of buses [2], [3]. In addition, due to the rapid and drastic fluctuation of renewable generation, the nodal voltage will change with the variation of power flows in the whole system, which could further jeopardize voltage security. Therefore, variability and uncertainty of renewable energy outputs have brought significant concerns over voltage security. In this paper, voltage security refers to the ability of power systems to withstand disturbances induced by uncertainties of renewable sources and contingencies of system assets without further loss of facilities or cascading failures [4]. Indeed, the optimal operation of power systems with a mix of heterogeneous energy sources always faces a tradeoff between security and economics, especially with an increasing penetration of renewables.

Indeed, pursuing higher economic efficiency would push power system assets operated closer to their limits, making them more vulnerable to outages and leading to lower security margins. Thus, system operators need to effectively manage the tradeoff between system security risks and economics when determining the optimal generation scheduling. A risk-averse stochastic unit commitment model is proposed while considering the loss-of-load risk induced by wind uncertainty [5]. A resilience-constrained unit commitment solution against cascading outages was developed in [6], by improving the homogeneity of power flow distribution and regulating power line loading rates against extreme weather events. In [7], a risk-averse two-stage stochastic optimization model was built by considering the conditional value-at-risk (CVaR) and the worst-case cost. In the above literature, expected unserved energy (EUE) was used as a risk index. However, EUE only measures load interruptions, but cannot accurately reflect the influence of volatility of renewables on other key operation state variables of power systems, such as nodal voltage.

Voltage security is defined as the capability of power systems in maintaining acceptable voltage magnitudes at all buses, under both normal and contingency conditions [8]. Various voltage security analysis methods have been explored for power systems with renewable energy penetration. A stochastic short-term AC security-constrained unit commitment model was proposed in [9] to demonstrate that unit commitment results can considerably affect bus voltage profiles. Thus, it is necessary to consider voltage security as an integral part of the power system operation scheduling study. To this end, in [10], operation constraints at the initial operation point as well as those at the voltage collapse point were considered simultaneously. Loading margin was employed in [11] as a voltage security index to guarantee the operation security of power systems. A multi-objective optimization framework was proposed in [12] while considering multiple security indices such as voltage drop index and voltage secu-

Y. Yin, T. Liu, and C. He are with the Department of Electrical Engineering, Sichuan University, Chengdu 610065, China (e-mail: yyin2016@126. com; tq-liu@scu.edu.cn; he_chuan@scu.edu.cn).

L. Wu (corresponding author) and Y. Liu are with the Department of Electrical and Computer Engineering, Stevens Institute of Technology, Hoboken, NJ 07030, USA (e-mail: lei.wu@stevens.edu; yliu262@stevens.edu).

rity margin. From the above literature review, the following points can be obtained.

1) Traditional optimal scheduling problems usually adopt simplified network models because of their computational advantages [13]. For instance, the optimal power flow (OPF) model usually adopts the DC power flow calculation [14], assuming a flat voltage magnitude for all buses and ignoring the reactive power. Losses in the DC OPF method are approximated via quadratic functions of bus angles [15], [16]. These oversimplified network models have several drawbacks: ① voltage security cannot be directly evaluated due to the lack of information on reactive power or voltage magnitude; ② the influence of reactive power on power flow calculation is ignored. Indeed, such simplified network models may increase operation costs, and even threaten security if power systems are operated in stressed status and/or have strong coupling between active and reactive power [17]. To this end, adopting accurate network models in the optimal scheduling problem would provide valuable information on system status to assess operation risks, and potentially save billions of dollars per year for power industry [18].

2) Risk indices adopted in [5]-[7], such as expected unserved energy, value-of-loss-of-load, and expected wind power curtailment, cannot reflect the influence of renewable energy volatility on certain key operation parameters of power systems, such as nodal voltage. Indeed, voltage is an essential indicator of system security, while maintaining voltage levels within a certain safe range and controlling voltage deviations of end users are among the primary tasks to ensure operation security of power systems. In power system operations, violations on transmission line capacity limits and voltage limits would pose direct and significant impacts on system security [19]-[21].

3) In order to maintain power system security, [10]-[12] restrict voltage deviations within a prespecified limit. In fact, renewable generation fluctuations usually occur in a short time period, while those significant ones are significantly rare. Therefore, applying strict voltage deviation limits could be overly conservative. In comparison, voltage risk assessment can accurately quantify damages to power systems [22]. As long as the overvoltage risk index of system is controlled under a tolerable range, the system security will be guaranteed, while the operation economics can also be greatly improved as compared to the conventional approach that adopts voltage deviation limits.

Due to uncertainty, variability, and hard-to-predict natures of renewable power outputs, comprehensive operation strategies of power systems are needed to ensure power system security while enhancing their effective utilization. To this end, cascading hydro units with fast response and storage capability could be used to economically compensate for uncertainties of wind and solar. However, since hydro units are greatly influenced by meteorological factors, thermal units, which are more reliable in operation and easier to dispatch, may still be indispensable in emerging power systems with a deeper penetration of renewables. Thus, this paper proposes a risk-constrained stochastic coordinated scheduling model of multi-energy system while considering economic and se-

cure operation against wind and solar uncertainties.

In the proposed coordinated scheduling model, a linearized AC power flow method [23] is employed, which can quantify the impacts of reactive power and voltage magnitude on real power dispatch. More importantly, voltage magnitudes are explicitly considered as state variables, and can be directly used to quantify system risks. The risk assessment method [24], [25] is used to analyze voltage security by quantitatively considering possibility and severity of voltage violations, which represents the economic losses in scenarios with different possibilities, and the factor of voltage security and economic factor can be linked to provide decision support in unit commitment. In practical operation, the system operator can determine the system overvoltage risk threshold via an offline assessment of overvoltage risks based on the predictions of wind and solar outputs [24], which will be incorporated into the proposed risk-constrained model. The proposed model is tackled via progressive hedging (PH) [26] by iteratively solving a set of subproblems for individual scenarios, and a relax-round-polish heuristic strategy is explored to enhance convergence performance.

The main contributions of this paper are as follows.

1) From the aspect of system modeling, the proposed risk-constrained stochastic optimization model formulates the coordinated scheduling of multi-energy system with uncertainties. Instead of DC power flow, linearized AC power flow model is used to explicitly formulate reactive power and voltage magnitude as decision variables.

2) From the aspect of risk quantification, overvoltage is used as a risk index, and the overvoltage risk constraint is integrated into the coordinated optimal scheduling model to leverage the latent scheduling capability of power systems with a mix of heterogeneous sources. To this end, the optimal solution represents a tradeoff between system operation economics and security with respect to a certain risk level.

3) From the aspect of algorithm, the risk-constrained stochastic optimization model is decomposed via PH to allow separate computation of individual scenarios. A relax-round-polish heuristic is embedded within the standard PH algorithm to improve the convergence performance of original stochastic problem with binary variables in both stages and obtain the high-quality suboptimal solutions.

The rest of the paper is organized as follows. Section II presents the risk-constrained stochastic model, and Section III discusses the risk-constrained coordinated scheduling of power systems with multiple sources. Sections IV details the solution methodology. Numerical case studies are presented in Section V, and the conclusions are given in Section VI.

II. RISK-CONSTRAINED STOCHASTIC MODEL

In order to achieve the environmental sustainability, and leverage the latent scheduling capacity of a multi-energy resource system, a risk-constrained stochastic optimization model is formulated for the coordinated scheduling of multi-energy system while considering uncertainties of renewable generation.

A. Severity Function for Security Evaluation of Voltage

It is critical for operation security of power systems to control voltage profiles and regulate reactive power. So voltage is usually considered as an important index to describe power quality, and reactive power balance is a basic premise to ensure voltage quality of power systems.

Overvoltage or undervoltage refers to that a nodal voltage exceeds its upper or lower limit. For the sake of discussion, the term overvoltage is used throughout the paper to represent both situations. If voltage exceeds the upper/lower limit, the system security would be compromised and system equipment would be damaged permanently. With respect to a given nodal voltage of bus i at time t, represented by $V_{i,t}$, equation (1) evaluates the severity of voltage outside its pre-specified limits in terms of the violation percentage [24].

$$\pi_{sev,V}\left(V_{i,t}\right)=\begin{cases}0 & 0.95\le V_{i,t}\le 1.05 \\ \dfrac{\mathrm{e}^{\Delta V_{i,t}}-1}{\mathrm{e}-1} & V_{i,t}<0.95 \text{ or } V_{i,t}>1.05\end{cases} \quad (1)$$

$$\Delta V_{i,t}=\begin{cases}0.95-V_{i,t} & V_{i,t}\le 0.95 \\ V_{i,t}-1.05 & V_{i,t}\ge 1.05\end{cases} \quad (2)$$

where $\Delta V_{i,t}$ is the voltage deviation of bus i at time t; and $\pi_{sev,V}(\cdot)$ is the severity function.

B. Overvoltage Risk Assessment Model

In a risk-constrained stochastic optimization problem, overvoltage risk refers to the expectation of overvoltage severity, computed as the summation of the product of overvoltage severities and the corresponding probabilities against various uncertainties and contingencies [24]. Uncertainties and contingencies are characterized via probabilistic representations. Specifically, by assigning the probabilities of individual scenarios $\Pr(\xi)$ to simulate renewable energy uncertainties and $\Pr\left(\boldsymbol{\Omega}^{\xi}\,|\,\xi\right)$ to describe the probabilities of distinct system statuses $\boldsymbol{\Omega}^{\xi}$ with respect to the individual contingencies in scenario ξ, the system overvoltage risk $\Lambda_{risk,V}\left(\boldsymbol{V}^{\xi},\boldsymbol{\Omega}^{\xi}\right)$ can be evaluated as (3). It is noteworthy that $\boldsymbol{\Omega}^{\xi}$ represents the set of system status in scenario ξ, which includes nodal voltages $\boldsymbol{V}^{\xi}$ and other system state variables. N_B and N_T are the numbers of buses and time periods, respectively.

$$\Lambda_{risk,V}\left(\boldsymbol{V}^{\xi},\boldsymbol{\Omega}^{\xi}\right)=\sum_{i=1}^{N_B}\sum_{t=1}^{N_T}\Pr\left(\boldsymbol{\Omega}^{\xi}\,|\,\xi\right)\pi_{sev,V}\left(V_{i,t}^{\xi}\right) \quad (3)$$

where $\Pr\left(\boldsymbol{\Omega}^{\xi}\,|\,\xi\right)=\Pr(\xi)/N^{\boldsymbol{\Omega}^{\xi}}$, $N^{\boldsymbol{\Omega}^{\xi}}$ is the number of $\boldsymbol{\Omega}^{\xi}$; and $V_{i,t}^{\xi}$ is the nodal voltage of bus i at time t in scenario ξ.

C. Optimization Model of Multi-energy System

A risk-constrained stochastic coordinated scheduling model of multi-energy system is studied to investigate the impacts of various uncertainties and contingences on system security. Notably, the multi-energy system is designed to operate with forecasted information, and thermal and hydro units would be adjusted adaptively against uncertainties and contingences while satisfying system risk constraints.

Multiple scenarios are generated to simulate wind and solar power output uncertainties with kernel density estimation [27], and the scenario reduction method [28] is applied to re-duce the number of scenarios to N_S as a tradeoff between calculation speed and solution accuracy.

The risk-constrained stochastic optimal scheduling model with N_S scenarios is presented in a general abstract form as (4)-(8). Binary variable equation (6) represents binary variable related constraints. System operation conditions in scenario ξ are presented as (7).

$$\min \boldsymbol{a}^{\mathrm{T}}\boldsymbol{x}+\sum_{\xi=1}^{N_S}\Pr\left(\xi\right)\left(\boldsymbol{e}^{\mathrm{T}}\boldsymbol{u}^{\xi}+\boldsymbol{c}^{\mathrm{T}}\boldsymbol{y}^{\xi}\right) \quad (4)$$

s.t.

$$\begin{cases}\boldsymbol{x}\in\{0,1\}^{N_X} \\ \boldsymbol{u}^{\xi}\in\{0,1\}^{N_U} \\ \boldsymbol{y}^{\xi}\in\mathbf{R}^{N_Y}\end{cases} \quad (5)$$

$$\begin{cases}\boldsymbol{A}\boldsymbol{x}\le\boldsymbol{d} \\ \boldsymbol{E}\boldsymbol{u}^{\xi}\le\boldsymbol{f}^{\xi}\end{cases} \quad (6)$$

$$\boldsymbol{C}\boldsymbol{x}+\boldsymbol{D}\boldsymbol{u}^{\xi}+\boldsymbol{F}\boldsymbol{y}^{\xi}\le\boldsymbol{z}^{\xi} \quad (7)$$

$$\sum_{\xi=1}^{N_S}\Pr\left(\xi\right)\Lambda_{risk,V}\left(\boldsymbol{V}^{\xi},\boldsymbol{y}^{\xi}\right)\le\varepsilon \quad (8)$$

where $\boldsymbol{x}$ is on/off status and startup/shutdown decisions; $\boldsymbol{u}^{\xi}$ and $\boldsymbol{y}^{\xi}$ are the auxiliary binary variables to linearize water-to-power conversion function and other system state variables in scenario ξ, respectively; $\boldsymbol{a}$, $\boldsymbol{c}$, $\boldsymbol{d}$, $\boldsymbol{e}$, $\boldsymbol{f}$, $\boldsymbol{z}$ are the coefficient vectors; $\boldsymbol{A}$, $\boldsymbol{C}$, $\boldsymbol{D}$, $\boldsymbol{E}$, $\boldsymbol{F}$ are abstract matrices; N_X, N_U, N_Y are the number of binary variables $\boldsymbol{x}$, $\boldsymbol{u}^{\xi}$, $\boldsymbol{y}^{\xi}$, respectively; and ε is the system overvoltage risk threshold, which can be set by system operators via an offline overvoltage risk assessment based on predictions of wind and solar outputs [24].

III. RISK-CONSTRAINED COORDINATED SCHEDULING OF THERMAL-HYDRO-WIND-SOLAR SYSTEMS

Considering that uncertainties of wind and solar energy outputs can compromise operation security of power systems, a risk-constrained multi-energy scheduling model is proposed to ensure the system security risk within a specific threshold. Specifically, overvoltage risk constraints are included to provide secure and cost-effective solutions against various uncertainties and contingences. Considering that many operation constraints, including branch power flow limits and voltage limits, are formulated as inequality constraints, over-limit risks of these operation constraints can be modeled using the similar approach for overvoltage risks adopted in this paper. Moreover, the impacts of these risk constraints on the system can be analyzed using the same algorithms presented in this paper. Thus, this paper focuses on the overvoltage risks for the detailed discuss, while other risk constraints, such as branch power flow over-limit risk assessment, could be added in the proposed model according to the demands of practical engineering application.

A. Objective Function

The objective of the proposed risk-constrained thermal-hydro-wind-solar scheduling problem is to minimize the expected system operation cost (9). The first term in (9) is the

startup/shutdown costs of thermal units, and the second term is the expected costs of multiple scenarios, including energy production cost of thermal units, penalty cost for energy spillage of wind-solar generation, and penalty cost of loss of load (LOL). To meet the overvoltage risk threshold, the optimal scheduling solution should comply with prevailing operation constraints, even under uncertainties, which are described in the following subsections.

$$\min \sum_{t=1}^{N_T}\left\{\sum_{g=1}^{N_G} C_g^{\text{fuel}}\left(A_{SU,g,t}+A_{SD,g,t}\right)+ \right.$$

$$\sum_{\xi=1}^{N_S}\Pr(\xi)\left[\sum_{g=1}^{N_G} C_g^{\text{fuel}} F_g\left(P_{g,t}^{\xi}\right)+\sum_{w=1}^{N_W} C_w\left(P_{w,t}^{\text{f},\xi}-P_{w,t}^{\xi}\right)+\right.$$

$$\left.\left.\sum_{s=1}^{N_{PV}} C_s\left(P_{s,t}^{\text{f},\xi}-P_{s,t}^{\xi}\right)+\sum_{d=1}^{N_L} C_d P_{LOL,d,t}^{\xi}\right]\right\} \tag{9}$$

where C_g^{fuel} is the fuel price of thermal unit g; $A_{SU,g,t}$ and $A_{SD,g,t}$ are the startup and shutdown indicators of thermal unit g at time t, respectively; $F_g(\cdot)$ is the function of energy consumption of thermal unit g; C_w, C_s, and C_d are the cost of renewable energy curtailment of wind farm w, solar power station s, and load shedding of load d, respectively; $P_{LOL,d,t}^{\xi}$ is the amount of LOL for load d at time t in scenario ξ; $P_{w,t}^{\text{f},\xi}$ and $P_{s,t}^{\text{f},\xi}$ are the forecasted power output of wind farm w and solar power station s at time t in scenario ξ, respectively; $P_{w,t}^{\xi}$ and $P_{s,t}^{\xi}$ are the active power dispatch of wind farm w and solar power station s at time t in scenario ξ, respectively; and N_L, N_G, N_W, N_{PV} are the number of loads, thermal units, wind farms and solar power stations, respectively.

B. System Constraints

System constraints include nodal power balance equations (10) and (11) and branch flow limits (12)-(14). AC power flow model is adopted to directly calculate bus voltages, reactive power, and network losses, which further enables system risk assessment.

1) Nodal power balance equations: constraints (10) and (11) describe active and reactive power balance equations of bus i. Constraints (10) and (11) contain squared voltage magnitude $\left(V_{i,t}^{\xi}\right)^2$, which is treated as a single variable (i.e., instead of $V_{i,t}^{\xi}$) in this paper.

$$\sum_{g\in i} P_{g,t}^{\xi}+\sum_{h\in i} P_{h,t}^{\xi}+\sum_{w\in i} P_{w,t}^{\xi}+\sum_{s\in i} P_{s,t}^{\xi}-\sum_{d\in i}\left(P_{d,t}^{\xi}-P_{LOL,d,t}^{\xi}\right)=$$

$$\sum_{(i,j)\in \Phi} P_{ij,t}^{\xi}+\left(\sum_{j=1}^{N_B} G_{ij,t}\right)\left(V_{i,t}^{\xi}\right)^2 \tag{10}$$

$$\sum_{g\in i} Q_{g,t}^{\xi}-\sum_{d\in i} Q_{d,t}^{\xi}=\sum_{(i,j)\in \Phi} Q_{ij,t}^{\xi}+\left(-\sum_{j=1}^{N_B} B_{ij,t}\right)\left(V_{i,t}^{\xi}\right)^2 \tag{11}$$

where $Q_{g,t}^{\xi}$ is the reactive power dispatch of thermal unit g at time t in scenario ξ; $P_{h,t}^{\xi}$ is the active power dispatch of hydro unit h at time t in scenario ξ; $P_{d,t}^{\xi}$ and $Q_{d,t}^{\xi}$ are the active and reactive power of load d at time t in scenario ξ, respectively; $P_{ij,t}^{\xi}$ and $Q_{ij,t}^{\xi}$ are the active and reactive power flow from bus i to bus j at time t in scenario ξ, respectively; G_{ij} and B_{ij} are the imaginary and real parts of the ith-row j^{th}-column element in admittance matrix, respectively; and Φ is

the set of branches.

2) Branch flow limits: real and reactive power flows on branch (i,j) are calculated as (12) and (13). Constraint (14) further describes the capacity limit of branch (i,j) in terms of apparent power allowance.

$$P_{ij,t}^{\xi}=g_{ij}\left[\left(V_{i,t}^{\xi}\right)^2-V_{i,t}^{\xi}V_{j,t}^{\xi}\cos\theta_{ij,t}^{\xi}\right]-b_{ij}V_{i,t}^{\xi}V_{j,t}^{\xi}\sin\theta_{ij,t}^{\xi} \tag{12}$$

$$Q_{ij,t}^{\xi}=-b_{ij}\left[\left(V_{i,t}^{\xi}\right)^2-V_{i,t}^{\xi}V_{j,t}^{\xi}\cos\theta_{ij,t}^{\xi}\right]-g_{ij}V_{i,t}^{\xi}V_{j,t}^{\xi}\sin\theta_{ij,t}^{\xi} \tag{13}$$

$$\left(P_{ij,t}^{\xi}\right)^2+\left(Q_{ij,t}^{\xi}\right)^2\leq\left(S_{ij}^{\max}\right)^2 \tag{14}$$

where b_{ij} and g_{ij} are the susceptance and conductance of branch (i,j), respectively; $\theta_{ij,t}^{\xi}$ is the phase angle difference between bus i and bus j at time t in scenario ξ; and $S_{ij}^{\max}$ is the apparent power limit of branch (i,j).

As the optimal scheduling problem is usually formulated as a mixed-integer linear programming (MILP) model by power system operators, nonlinear terms in constraints (12)-(14) are reformulated via the Taylor series expansion and the piecewise linearization method, respectively. The detailed procedures are presented in Appendix A.

In this paper, a linearized AC power flow is adopted, as shown in Appendix A. The linearized AC power flow model assumes that $\theta_{ij,t}^{\xi}$ is small, thus sine and cosine functions can be approximated as (A1). In addition, voltage magnitudes of all buses are assumed close to 1.0 p.u., thus (A2) is further applied to decouple the voltage magnitude and angle.

C. Thermal Unit Constraints

Thermal unit constraints include capacity limits (15) and (16), power factor limit (17), minimum on/off time limits (18) and (19), startup and shutdown costs (20) and (21), and ramp up and down limits (22) and (23).

$$P_g^{\min} I_{g,t}\leq P_{g,t}^{\xi}\leq P_g^{\max} I_{g,t} \tag{15}$$

$$Q_g^{\min} I_{g,t}\leq Q_{g,t}^{\xi}\leq Q_g^{\max} I_{g,t} \tag{16}$$

$$-\left(\tan\sigma_g\right)P_{g,t}^{\xi}\leq Q_{g,t}^{\xi}\leq\left(\tan\sigma_g\right)P_{g,t}^{\xi} \tag{17}$$

$$\left(X_{g,(t-1)}^{\text{on}}-T_g^{\text{on}}\right)\left(I_{g,(t-1)}-I_{g,t}\right)\geq 0 \tag{18}$$

$$\left(X_{g,(t-1)}^{\text{off}}-T_g^{\text{off}}\right)\left(I_{g,t}-I_{g,(t-1)}\right)\geq 0 \tag{19}$$

$$A_{SU,g,t}\geq A_{SU,g}\left(I_{g,t}-I_{g,(t-1)}\right)\quad A_{SU,g,t}\geq 0 \tag{20}$$

$$A_{SD,g,t}\geq A_{SD,g}\left(I_{g,(t-1)}-I_{g,t}\right)\quad A_{SD,g,t}\geq 0 \tag{21}$$

$$P_{g,t}^{\xi}-P_{g,(t-1)}^{\xi}\leq\varsigma_{UR,g}I_{g,(t-1)}+P_g^{\min}\left(I_{g,t}-I_{g,(t-1)}\right)+P_g^{\max}\left(1-I_{g,t}\right) \tag{22}$$

$$P_{g,(t-1)}^{\xi}-P_{g,t}^{\xi}\leq\varsigma_{UD,g}I_{g,t}+P_g^{\min}\left(I_{g,(t-1)}-I_{g,t}\right)+P_g^{\max}\left(1-I_{g(t-1)}\right) \tag{23}$$

where $P_g^{\max}$ and $P_g^{\min}$ are the maximum and minimum real power of thermal unit g, respectively; $Q_g^{\max}$ and $Q_g^{\min}$ are the maximum and minimum reactive power of thermal unit g, respectively; $A_{SU,g}$ and $A_{SD,g}$ are the startup and shutdown indicators of thermal unit g, respectively; $I_{g,t}$ and $I_{g(t-1)}$ are the

commitment statuses of unit g at time t and $t-1$, respectively; σ_g is the power angle limit of unit g; T_g^{on} and T_g^{off} are the minimum on/off time of thermal unit g, respectively; $X_{g,t}^{\text{on}}$ and $X_{g,t}^{\text{off}}$ are the on/off time counters of thermal unit g at time t, respectively; $\varsigma_{UD,g}$ and $\varsigma_{UR,g}$ are the ramp down and up rates of thermal unit g, respectively.

D. Cascading Hydro Unit Constraints

Capacity limits, minimum on/off time limits, and ramp up and down limits of hydro unit h can be similarly formulated as those in (15), (18)-(21) and (22)-(23). In addition, constraints (24)-(26) are unique for cascading hydro units.

Constraint (24) ensures water balance of cascading hydro units. It assumes that hydro unit $(h-1)$ is on the upstream of hydro unit h, and it takes τ hours for the water discharged from hydro unit $(h-1)$ to arrive at hydro unit h. Water discharge limits and reservoir volume limits are expressed via (25) and (26), respectively.

$$R_{h,t}^{\xi} = R_{h,(t-1)}^{\xi} + r_h + L_{(h-1),(t-\tau)}^{\xi} - L_{h,t}^{\xi} \tag{24}$$

$$L_h^{\min} I_{h,t} \le L_{h,t}^{\xi} \le L_h^{\max} I_{h,t} \tag{25}$$

$$\begin{cases} R_h^{\min} \le R_{h,t}^{\xi} \le R_h^{\max} \\ R_h^0 = R_{h,0}^{\xi} \\ R_h^{N_T} = R_{h,N_T}^{\xi} \end{cases} \tag{26}$$

where $R_{h,t}^{\xi}$ and $R_{h,(t-1)}^{\xi}$ are the reservoir volumes of hydro unit h at time t and time $t-1$ in scenario ξ, respectively; r_h is the natural water inflow to reservoir of hydro unit h; $L_{h,t}^{\xi}$ is the water discharge of hydro unit h at time t in scenario ξ; $L_h^{\max}$ and $L_h^{\min}$ are the maximum and minimum discharge of hydro unit h, respectively; $R_h^{\max}$ and $R_h^{\min}$ are the maximum and minimum reservoir volumes of hydro unit h, respectively; $I_{h,t}$ is the commitment status of hydro unit h at time t; and R_h^0 and $R_h^{N_T}$ are the initial and terminal reservoir volumes of hydro unit h, respectively.

Water-to-power conversion of cascading hydro units is described via a head-dependent function (27), where water head level $H_{h,t}^{\xi}$ is a function of reservoir volume, i.e., $H_{h,t}^{\xi} = h_h^0 + \alpha_h R_{h,t}^{\xi}$, where h_h^0 and α_h are the coefficients dependent on physical characteristics of reservoir of hydro unit h.

$$P_{h,t}^{\xi} = \eta_h L_{h,t}^{\xi} H_{h,t}^{\xi} \tag{27}$$

where η_h is the water-to-power conversion coefficient of hydro unit h.

Thus, the head-dependent water-to-power conversion function is given as in (28).

$$P_{h,t}^{\xi} = \eta_h L_{h,t}^{\xi} \left(h_h^0 + \alpha_h R_{h,t}^{\xi} \right) \tag{28}$$

E. Solar and Wind Power Constraints

Operation constraints of wind farms and solar farms are expressed as (29) and (30), which describe that dispatches of wind and solar power at time t do not exceed their forecasting values [29]-[31].

$$0 \le P_{w,t}^{\xi} \le P_{w,t}^{f,\xi} \tag{29}$$

$$0 \le P_{s,t}^{\xi} \le P_{s,t}^{f,\xi} \tag{30}$$

F. Risk Constraints

To ensure system operation security, the optimal scheduling model also includes overvoltage risk constraint (8).

IV. Solution Methodology

The proposed risk-constrained day-ahead scheduling problem is a two-stage stochastic programming model with binary variables in both stages, and is formulated as an MILP model. PH is a scenario-based decomposition technique that can be leveraged to solve such problems effectively. Indeed, PH can serve as a heuristic approach to solve two-stage stochastic programming problems with integer decision variables in both stages [26]. Since the number of iterations required is frequently impractical for complex non-convex stochastic integer programming problems, a relax-round-polish approach is also presented to enhance convergence performance while obtaining high-quality suboptimal solutions.

A. PH-based Decomposition Approach

In the risk-constrained stochastic optimization problem (4)-(8), the first-stage decision x implements the non-anticipativity requirement to force that unit commitment decisions are scenario-independent. Binary variables u^{ξ} and continuous variables y^{ξ} represent second-stage scenario-specific decisions. Constraints (5)-(8) are expressed as $(x, u^{\xi}, y^{\xi}) \in \Psi_{\xi}$ for the sake of discussion.

The basic PH algorithm is stated as follows.

Step 1: initialize parameters. Set iteration index $\vartheta = 0$, penalty factor $\varrho > 0$, penalty term $\omega_{\xi}^{\vartheta} = 0$, and termination threshold $\Gamma = 0.001$.

S*tep 2*: solve subproblems. Calculate subproblems of individual scenarios, $x_{\xi}^{\vartheta} = \arg\min_{x,y^{\xi}} \left(a^{\mathrm{T}} x + e^{\mathrm{T}} u^{\xi} + c^{\mathrm{T}} y^{\xi} \right): \left(x, y^{\xi} \right) \in \Psi_{\xi}$, obtain $\bar{x}^{\vartheta}$ and the penalty term ω_{ξ}^{ϑ} as $\bar{x}^{\vartheta} = \sum_{\xi=1}^{N_S} \Pr(\xi) x_{\xi}^{\vartheta}$ and $\omega_{\xi}^{\vartheta} = \varrho \left(x_{\xi}^{\vartheta} - \bar{x}^{\vartheta} \right)$, respectively.

Step 3: update penalty term. Update iteration index $\vartheta = \vartheta + 1$, solve subproblems of individual scenarios, $x_{\xi}^{\vartheta} = \arg\min_{x,y^{\xi}} \left(a^{\mathrm{T}} x + e^{\mathrm{T}} u^{\xi} + c^{\mathrm{T}} y^{\xi} + \omega_{\xi}^{\vartheta-1} x + \varrho \left\| x - \bar{x}^{\vartheta-1} \right\|^2 / 2 \right): \left(x, y^{\xi} \right) \in \Psi_{\xi}$, update $\bar{x}^{\vartheta}$ and the penalty term ω_{ξ}^{ϑ} as $\bar{x}^{\vartheta} = \sum_{\xi=1}^{N_S} \Pr(\xi) x_{\xi}^{\vartheta}$ and $\omega_{\xi}^{\vartheta} = \omega_{\xi}^{\vartheta-1} + \varrho \left(x_{\xi}^{\vartheta} - \bar{x}^{\vartheta} \right)$.

Step 4: convergence check. Calculate primal residue ϖ^{ϑ} as $\varpi^{\vartheta} = \sum_{\xi=1}^{N_S} \left\| \Pr(\xi) x_{\xi}^{\vartheta} - \bar{x}^{\vartheta} \right\|$, if $\varpi^{\vartheta} \le \Gamma$, the final optimal solution is obtained; otherwise, go to *Step 3*.

B. Relax-round-polish Based Improvement of PH Algorithm

Through the above iterative procedure, PH may eventually force the consensus among decision variables x^{ξ} of individual scenarios to a common value x. It is noteworthy that binary variables u^{ξ} included in the second stage of problem (4) may compromise convergence performance of the PH algorithm [26]. An improved PH is adopted to enhance convergence performance of this problem, which is a heuristic approach including the relax-round-polish procedure. The main

idea is to solve the relaxed scenario subproblems using basic PH, identify an integer feasible solution in the neighborhood of the solution obtained from the relaxed scenario subproblems via objective feasibility pump, and improve the feasible solution by an iterative local search [32].

The procedure of the improved PH is as follows.

Step 1: set iteration index $\vartheta = 0$; *Step 2* of the basic PH is executed to solve subproblems of individual scenarios, and calculate $\bar{x}^{\vartheta}$.

Step 2: initialize $k = 1$; for the current solution $\bar{x}^{\vartheta}$, for $\forall i \in \{1, 2, ..., N_X\}$: if $\bar{x}_i^{\vartheta} = 0$, set $\tilde{x}_{\xi,i}^k = 0$ for $\forall \xi \in \{1, 2, ..., N_S\}$; if $\bar{x}_i^{\vartheta} = 1$, set $\tilde{x}_{\xi,i}^k = 1$ for $\forall \xi \in \{1, 2, ..., N_S\}$. Sort all the remaining $\bar{x}_i^{\vartheta}$ as $\bar{x}_1^{\vartheta} \geq \bar{x}_2^{\vartheta} \geq ... \geq \bar{x}_{N_{nub}}^{\vartheta} \geq x_{UB} \geq ... \geq x_{LB} \geq \bar{x}_{N_{ni}-f}^{\vartheta} \geq ... \geq \bar{x}_{N_{ni}}^{\vartheta}$. x_{UB} and x_{LB} are the upper and lower bounds used in the relax-round-polish procedure; N_{ni} is the number of remaining $\bar{x}_i^{\vartheta}$ whose solutions are non-integer values; N_{nub} is the number of the remaining $\bar{x}_i^{\vartheta}$ whose solutions are no smaller than x_{UB}; f is the number of the remaining $\bar{x}_i^{\vartheta}$ whose solutions are no larger than x_{LB}.

Step 3: set $\tilde{x}_i^k = 1$ for $\forall i \in \{1, 2, ..., N_{nub}\}$, and set $\tilde{x}_j^k = 0$ for $\forall j \in \{N_{ni} - f, N_{ni} - f + 1, ..., N_{ni}\}$.

Step 4: check the feasibility of individual subproblems by fixing binaries x according to $\tilde{x}^k$.

Step 5: if the solution is integer-infeasible, release a pair of $\tilde{x}_i^k$ and $\tilde{x}_j^k$ whose indices are the largest (i.e., free two variables whose solutions are closest to x_{UB} and x_{LB}, respectively); set $k = k + 1$, $\tilde{x}_{\xi,i}^k = \tilde{x}_{\xi,i}^{k-1}$ for $\forall i \in \{1, 2, ..., N_{nub} - 1\} \cup \{N_{ni} - f + 1, N_{ni} + f + 2, ..., N_{ni}\}$, set $N_{nub} = N_{nub} - 1$ and $f = f - 1$, and go back to *Step 4*; if an integer feasible solution is found, set $\hat{x}^{\vartheta+1} = \tilde{x}^k$ and go to *Step 6*.

Step 6: set iteration index $\vartheta = \vartheta + 1$, and solve the subproblems corresponding to *Step 3* of basic PH with part of binary variables x fixed according to $\hat{x}^{\vartheta+1}$.

Step 7: check convergence. If binary solutions do not change or $\varpi^{\vartheta} \leq \Gamma$, terminate; otherwise, go to *Step 2*.

C. Procedure of Proposed Approach

The procedure of the proposed stochastic coordinated scheduling model, as shown in Fig. 1, is summarized as follows.

Step 1: ten thousand scenarios are generated to simulate wind and solar power output uncertainties via kernel density estimation [28], [33].

Step 2: scenario reduction technique is implemented to obtain a small number of representative scenarios, as a tradeoff between computation speed and result accuracy [28], [33].

Step 3: solve the proposed stochastic coordinated scheduling model with improved PH decomposition approach. The detailed procedure of the improved PH is shown in Section IV, Part A and B. It is noticed that the nonlinear head-dependent water-to-power conversion function (28) is piecewise linearized [28], which can be incorporated into the MILP model. The piecewise linear reformulation of (28) is presented in Appendix A.
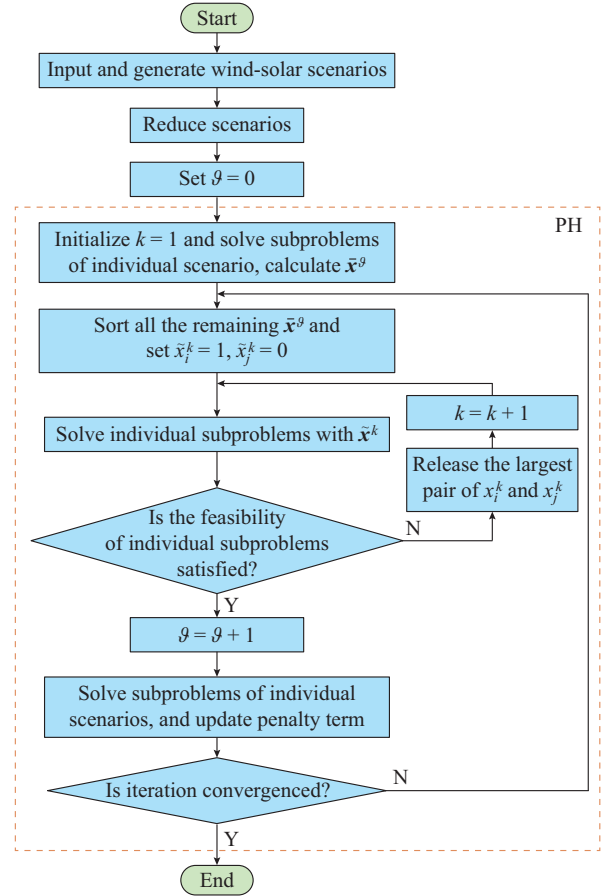

Fig. 1. Flowchart of proposed model.

V. CASE STUDIES

In this section, the effectiveness of the proposed method is tested via a modified IEEE 30-bus system and a modified IEEE 118-bus system. Numerical simulations are implemented by Gurobi 6.5 on a personal computer. Cost coefficients of electrical load shedding and wind and solar spillage are set as 6600 \$/MWh [34] and 100 \$/MWh [35], respectively.

A. IEEE 30-bus System

The modified IEEE 30-bus system includes 6 thermal units (G1, G2, ..., G6), 41 transmission lines, and 20 loads. The network topology of the modified IEEE 30-bus system is shown in Fig. 2. Generator and transmission line data are obtained from MatPower 4.1 [36]. Two hydro units H1 and H2 in a cascading hydro system are connected to buses 6 and 8, respectively. Each of buses 11 and 25 includes one wind farm and one solar generation station (WS), notably WSII and WSI, respectively. The forecasting values of electrical load, wind and solar generation are shown in Fig. 3 with respective peak values of 241 MW, 72 MW, and 30 MW that do not occur simultaneously. At the peak-load period, wind and solar generation accounts for about 30% of the total power generation. Data of the thermal units and hydro units are shown in Appendix A Tables AI-AIII. Data of wind and solar generation can be referred from [33]-[37]. Table I shows the probabilities of the scenarios.
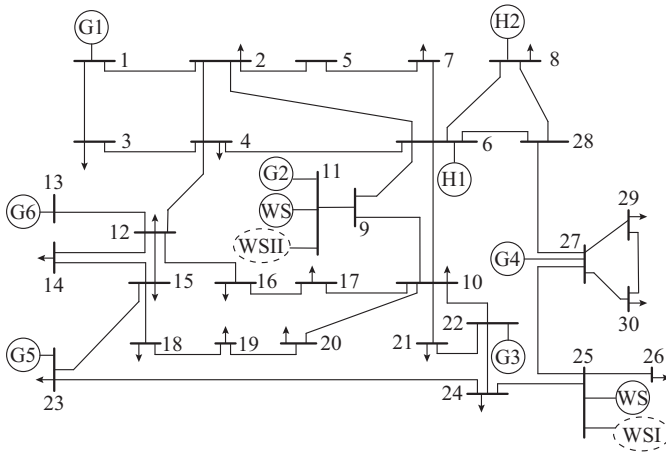
The following four cases are studied.
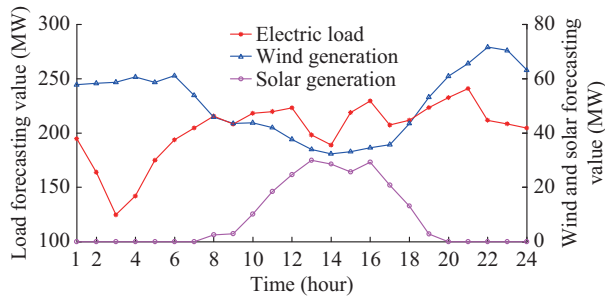
Fig. 2. Modified IEEE 30-bus system.

Fig. 3. Forecasting values of electrical load as well as wind and solar generation.

TABLE I
PROBABILITIES OF SCENARIOS

Scenario	Probability	Scenario	Probability
1	0.0098	6	0.3692
2	0.0021	7	0.0012
3	0.0099	8	0.1753
4	0.3369	9	0.0045
5	0.0349	10	0.0562

Case 1: analyzing the accuracy of the linearized AC power flow model against the DC power flow model.

Case 2: studying the effects of overvoltage risk constraints and different renewable penetration levels.

Case 3: investigating the impacts of locations of renewable energy.

Case 4: exploring the impacts of extreme weather situations on cascading hydro unit operation and system security.

In Case 1, compared to the DC power flow model, three models are used to analyze the accuracy of the linearized AC power flow model adopted in this paper.

Three models are compared to show the advantages of the linearized AC power flow model. PF(I) is a full AC power flow model performed via MatPower, with fixed active and reactive power injections of PQ buses as well as the voltage angle and magnitude of the swing bus; PF(II) is the commonly used DC power flow model [28], [29]; PF(III) is the linearized AC power flow model adopted in this paper, with

initial magnitudes and angles of bus voltages set as 1 p.u. and 0 p.u., respectively. The power flows in PF(I), PF(II), and PF(III) are compared in Fig. 4. The maximum absolute error in the power flows between PF(I) and PF(III) is 0.0604 p.u., which is much smaller than that between PF(I) and PF(II). To this end, a smaller error indicates that the linearized AC power flow model is more accurate than the DC power flow model. In addition, PF(III) explicitly includes system reactive power and voltage variables, which can facilitate the overvoltage risk assessment.
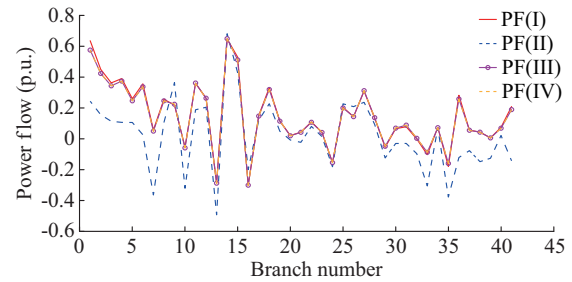

Fig. 4. Comparison of different power flow models in Case 1.

In order to further understand the impact of the initial voltage magnitude and angle values on the power flow calculation, PF(IV) is executed by setting the initial values of bus voltages and angles as the final AC power flow solution obtained from PF(I). The absolute errors of the real power, reactive power, and nodal voltage of PF(III) and PF(IV) against PF(I) are enumerated in Table II. Table II shows that, although initial values of PF(IV) and PF(III) are different, the absolute errors of the active power, reactive power, and voltage between PF(IV) and PF(I) are 0.0603 p.u., 0.0808 p.u., and 0.0206 p.u., respectively, which are very close to 0.0604 p.u., 0.0859 p.u., and 0.0207 p.u. obtained from PF(III). This clearly shows that the linearized AC power flow approach has a wide convergence range, and the initial setting of 1.0 p.u. and 0 p.u. for voltage magnitude and angle will not result in significant errors in power flow results.

TABLE II
COMPARISON OF PF(III) AND PF(IV) IN CASE 1

Powe flow model	Maximum absolute error (p.u.)			Solution time (s)
	Active power	Reactive power	Voltage	
PF(III)	0.0604	0.0859	0.0207	3
PF(IV)	0.0603	0.0808	0.0206	2

In Case 2, The effects of overvoltage risk constraints and different renewable penetration levels on the coordinated scheduling of the mix of energy sources are studied.

1) The intermittent nature of renewable energy will significantly impact voltage profiles of the power system. Specifically, if voltage constraints are not considered, the solutions to the stochastic coordinated scheduling model derive a voltage risk index value of 2.50×10^{-3}, and the most vulnerable nodes are buses 10, 13, 22, and 30. Statistical analysis on voltage profiles of the four buses is reported in Table III. It

shows that due to the uncertainties of wind-solar outputs, overvoltage events occur 229 times on bus 13 in all 10 scenarios throughout the 24 hours. The mean voltage level of bus 13 is 1.0970 p.u., with the maximum and minimum values of 1.1 p.u. and 1.0396 p.u., respectively. The unit commitment results of thermal units G1-G6 are shown in Fig. 5(a) with the total operation cost of $176,194.43.

TABLE III
ANALYSIS OF SYSTEM VOLTAGE WITHOUT CONSIDERING VOLTAGE LIMIT

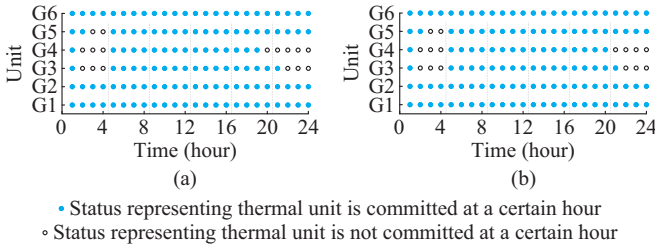| Bus	Minimum value of voltage (p.u.)	Maximum value of voltage (p.u.)	Mean value of voltage (p.u.)	Standard deviation of voltage (p.u.)	Number of over-voltage
10	0.9918	1.0694	1.0529	0.0133	133
13	1.0396	1.1000	1.0970	0.0111	229
22	0.9213	0.9896	0.9521	0.0226	94
30	0.9041	0.9787	0.9362	0.0227	147

Fig. 5. Unit commitment solution of Case 2. (a) Unit commitment with overvoltage risks. (b) Unit commitment with voltage limits.

The stochastic coordinated scheduling models with the overvoltage risk constraints (i.e., overvoltage risk threshold is set as 1×10^{-4} [38], [39]) and the nodal voltage limits (i.e., voltage limit is set as [0.95, 1.0]p.u.) are executed. The unit commitment results with overvoltage risk constraints are the same as Fig. 5(a). However, due to the overvoltage risk constraints, the total energy production of thermal unit G4 is reduced from 562.96 MWh to 554.83 MWh, replaced by the more expensive thermal unit G5. G5 is committed to ensure enough reactive power for supporting voltage profiles, to meet overvoltage risk constraints and support active power transfer. The unit commitment results with voltage limits are shown in Fig. 5(b). Compared with Fig. 5(a), thermal unit G4 is committed for one more hour (i.e., at the 20th hour) for the same reason.

As observed in Table IV, the total cost with overvoltage risk constraints is $377.31 less than that with voltage limit, while the mean and standard deviations of nodal voltage magnitudes are at the similar level. Therefore, considering overvoltage risk constraints can ensure voltage security and improve economic operation of systems.

2) Four penetration levels of 20%, 25%, 35%, and 40% are tested. The total cost is decreased from $191229.58 with 20% penetration level to $169715.36 with 40% penetration level. The total energy produced from thermal units is reduced from 5744.30 MWh to 5145.79 MWh. On the other hand, the overvoltage risk index of the power system is increased from 1.46×10^{-3} to 1.06×10^{-2}. Statistical analysis on

the most vulnerable nodes are enumerated in Table V. It indicates that with the increase of the penetration level of wind-solar generation, the reliance of the power system on thermal units and the system operation cost are both reduced, at the cost of a higher overvoltage risk of the system.

TABLE IV
ANALYSIS ON IMPACT OF OVERVOLTAGE RISK CONSTRAINTS AND VOLTAGE LIMIT

Constraint and limit	Mean value of voltage (p.u.)	Standard deviation of voltage (p.u.)	Total cost ($)
Without overvoltage risk constraints and voltage limit	1.0085	0.0317	176194.43
With overvoltage risk constraints	1.0140	0.0306	176204.64
With voltage limit	1.0226	0.0330	176581.95

TABLE V
ANALYSIS OF SYSTEM VOLTAGE OF DIFFERENT BUSES

Penetration level (%)	Bus number	Mean value of voltage (p.u.)	Standard deviation of voltage (p.u.)
20	10	0.9479	0.0212
	13	0.9495	0.0322
	22	0.9535	0.0228
	30	0.9453	0.0227
25	10	1.0530	0.0141
	13	1.0945	0.0130
	22	0.9546	0.0219
	30	0.9388	0.0222
35	10	1.0497	0.0230
	13	1.0891	0.0370
	22	0.956	0.0212
	30	0.9402	0.0212
40	10	1.0471	0.0351
	13	1.0790	0.0527
	22	0.9627	0.0232
	30	0.9470	0.0232

Using the overvoltage risk index threshold of 1.00×10^{-4}, the mean and standard deviation of voltages among all scenarios during 24 hours are enumerated in Table VI. The mean and standard deviations of voltages with penetrations are about 1.01 p.u. and 0.03 p.u., respectively, representing a relatively better voltage profile as compared to the results without overvoltage risk constraints.

It is also observed that the rate of system cost reduction is decreased with the increase in the penetration level, as shown in Fig. 6. Especially, when the wind-solar power penetration increases from 35% to 40%, the rate of system cost reduction is only 0.36%. The reason is that when the penetration of wind and solar reaches a critical level, the capability of the system in absorbing renewable energy becomes weakened as constrained by overvoltage risk limits. Meanwhile, it is observed that the cost difference caused by voltage constraint enlarges with the increase in the penetration level of wind and solar generation.

The spillage of wind and solar energy is shown in Fig. 7. With overvoltage risk constraints, the amount of wind and solar energy spillage at the penetration level of 35% is 13.09 MWh, which is 32.70% less than that at the penetration level of 40%. That is, the renewable energy utilization efficiency at the penetration level of 35% is higher than that at the penetration level of 40%. In order to balance the efficiency of renewable energy utilization and security operation of the system, the penetration level of wind and solar generation should be appropriately leveraged according to the system overvoltage risk tolerance.

TABLE VI
ANALYSIS OF SYSTEM VOLTAGE WITH DIFFERENT PENETRATION LEVELS

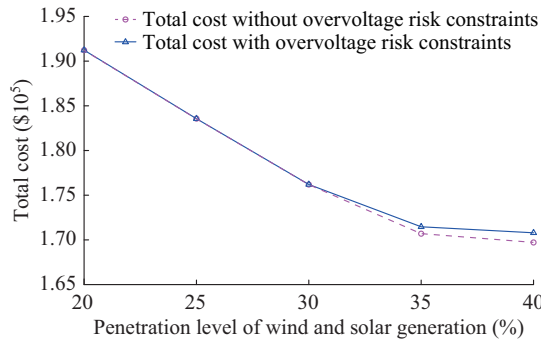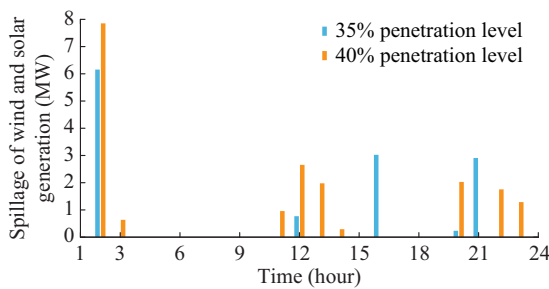| Penetration level (%)	Mean value of voltage (p.u.)	Standard deviation of voltage (p.u.)	Number of overvoltage
20	1.0120	0.0295	92
25	1.0105	0.0310	94
30	1.0140	0.0311	94
35	1.0145	0.0293	94
40	1.0101	0.0261	95

Fig. 6.   Total cost.

Fig. 7.   Spillage of wind and solar generation at different penetration levels.

In Case 3, the impact of locations of wind and solar power plants on operation security of power systems is analyzed. Specifically, one more set of wind farm and solar generation station is deployed in the system with the same energy output characteristics as shown in Fig. 3.

The severity indices of overvoltage are shown in Fig. 8. Although the penetration levels are the same, the system overvoltage risk index values are different. In contrast, the overvoltage risk index is 1.77×10^{-2} in WSI, which is much higher than that of 5.57×10^{-3} in WSII. The total cost in WSI is $165469.54, which is also significantly higher than that of $133879.11 in WSII.
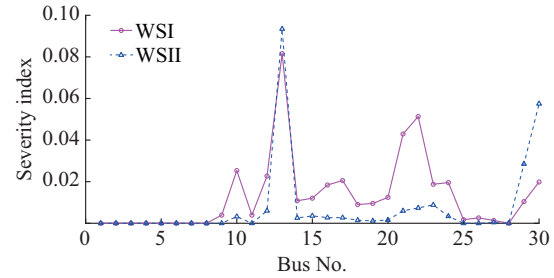

Fig. 8.   Severity indices of overvoltage for Case 3.

In Fig. 8, buses 10, 13, 22, and 30 show severe overvoltage, where the severity index of WSI is larger than that of WSII. The reason is that the active power dispatches of G3 and G6 have to be increased to compensate the fluctuation of wind and solar generation, and active power transfer requires reactive power support. Thus, there is serious overvoltage at buses 22 and 13 (i.e., where G3 and G6 are located, respectively) due to the excessive reactive power. For the same reason, the reactive power of G3 mainly supports active power transfer from bus 22 to bus 24, and overvoltage occurs at bus 10 due to reactive power deficiency. The situation on bus 30 can be analyzed similarly.

1) When the overvoltage risk constraint is considered with the limit of 1.00×10^{-4}, the total cost is shown in Table VII. The total cost of WSI is $166789.38, which is higher than that of WSII. The reason is that the total dispatch of G2, which is the most expensive unit, is increased from 848.22 MWh in WSII to 1112.74 MWh in WSI for improving system voltage profile. Thus, in order to improve the efficiency of renewable energy utilization, the local consumption should be encouraged as much as possible, or the renewable energy and traditional units should be bundled as in WSII (i.e., thermal unit G2 is collocated at bus 11).

TABLE VII
RESULTS WITH DIFFERENT CALCULATION CONDITIONS

Calculation condition	Mean value of voltage (p.u.)		Standard deviation of voltage (p.u.)		Total cost ($)	
	WSI	WSII	WSI	WSII	WSI	WSII
Overvoltage risk	0.9933	0.9971	0.0202	0.0204	166789.38	136774.04
DC power flow	1.0079	1.0178	0.0241	0.0265	170025.95	138634.95

2) The scheduling model is implemented with DC power flow model. The total costs for WSI and WSII are $129936.77 and $109962.82, respectively, which are both smaller than those with AC power flow model and overvoltage risk constraints. The unit commitment solutions with DC power flow are then applied to those with overvoltage risk

constraints to further calculate their corresponding optimal economic dispatch (ED) solutions. The results of ED solutions show that for WSI, the total cost is increased to $174148.69, with $4646.65 for renewable generation curtailment; for WSII, the total cost is increased to $138972.26 with $2725.91 for renewable generation curtailment. The results show that renewable energy spillage with overvoltage risk constraints for WSI and WSII are 4.43% and 9.67% less than those with DC power flow, respectively. Thus, the solution of Case 3 with overvoltage risk constraints is more reliable against the fluctuations of wind and solar generation.

3) Case 3 is further implemented with voltage limit. The results are shown in Table VII. With the consideration of voltage limit, the voltage profile is always kept in [0.95, 1.0] p.u.. The mean voltage for WSI and WSII are 1.0079 p.u. and 1.0178 p.u., respectively. The standard deviation of voltages in for WSI and WSII are 0.0241 p.u. and 0.0265 p.u., respectively. For WSI, the differences of mean voltage and standard deviation between overvoltage risk constraint and voltage limit are 0.0146 p.u. and 0.0039 p.u., respectively. For WSII, the difference of mean voltage and standard deviation considering between overvoltage risk constraints and DC powe flow model are 0.0207 p.u. and 0.0061 p.u., respectively. In addition, the total costs with voltage limit for WSI and WSII are $170025.95 and $138634.95, respectively, which are 1.94% and 1.36% higher than those with overvoltage risk constraint, respectively. It shows that when voltage limit is considered, the system voltage profile with voltage limit is improved at the cost of slight compromise in system operation economics.

Case 4: the impact of a severe weather condition is studied, i.e., a dry season with low water inflows to the cascading system. The natural inflows of H1 and H2 are set as 0.6 Hm^3/h and 0.9 Hm^3/h, respectively, which are 30% of the original data used in Case 2.

Because of the fast response capability and operation economics, hydro power is considered as a valuable resource for compensating uncertainties of wind and solar generation. However, fast response capacity of hydro units is greatly influenced by meteorological factors. In Case 4, due to the limited natural water supply, such capabilities of hydropower units are replaced by thermal units. Without overvoltage risk constraints, the overvoltage risk index of Case 4 is 1.58×10^{-2}, which is higher than that of Case 2. The minimum and maximum voltage values across all scenarios in Case 4 are 1.1 p.u. and 0.9247 p.u., respectively. Standard deviation of Case 4 is 0.0380 p.u., as compared to 0.0317 p.u. in Case 2. Hourly dispatches of H1 and H2 are shown in Fig. 9.

It indicates that hydro units are mainly dispatched as peaking units in dry seasons, in order to effectively use limited water resources. Thermal units, which feature reliable operation and strong dispatchability, will still be important power sources, as limited outputs of hydro units will be partially replaced by thermal units to meet loads and mitigate uncertainties of renewable energy.

In this system, the transmission line connecting buses 6 and 9 plays a vital role in energy delivery. Figure 10 shows the power flow of this line. As can be seen, in Case 2, reservoirs of hydro units have sufficient water inflow and certain storage capacity, thus can fully execute their fast response capabilities. Power flows from node 6 to node 9 are positive with relatively large values during hours 1-6, 13, 14, and 22-24, which means hydro units have sufficient power to compensate uncertainties of wind and solar generation, besides supplying the loads located at bus 8. However, when water is limited in Case 4, the flexibility of hydro units is weakened, and thermal units become a reliable choice to compensate the uncertainty of wind-solar generation, especially during hours 1-6, 13, 14, and 22-24. Power flow direction of this transmission line is changed in these hours, indicating that the thermal units are committed to compensate hydropower generation shortage. In this case, thermal units G1-G4 are all committed throughout the day. The total dispatch of thermal units is increased from 5307.80 MWh in Case 2 to 5787.00 MWh in Case 4. The total cost is $224598.23.
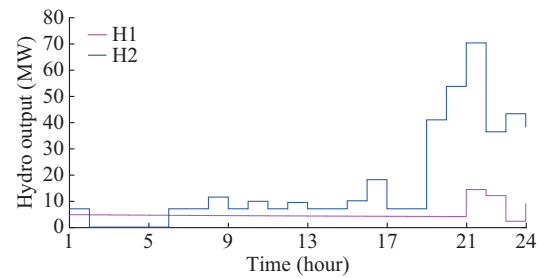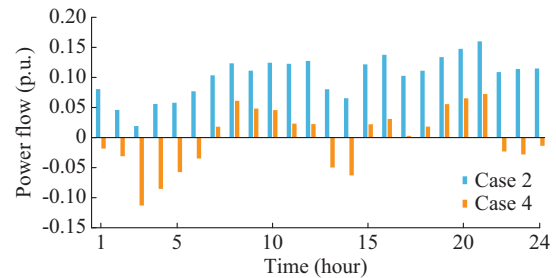

Fig. 9. Hourly dispatches of H1 and H2.

Fig. 10. Comparison of power flow from bus 6 to bus 9.

1) Further adopting overvoltage risk constraints (with the same limit of 1.00×10^{-4} used in Case 2) can improve the voltage profile. The maximum and minimum magnitudes of voltage are 1.0877 p.u. and 0.9327 p.u., respectively. The mean magnitude of voltage for the most vulnerable buses 10, 13, 22, and 30 are 1.0338 p. u., 1.0552 p. u., 1.0472 p. u., and 0.9425 p. u., and their standard deviations are 0.0125 p. u., 0.0117 p. u., 0.0170 p. u., and 0.0070 p. u., respectively. Moreover, with the increase in the dispatch of G2, the total cost is $245346.92, including $15320.31 penalty of LOL and $41990.79 penalty of wind and solar spillage.

2) Case 4 is implemented with DC power flow model. The total cost is $191950.47, which is 27.82% lower than those with overvoltage risk constraints. By comparison, the set of unit commitment solutions to adopting overvoltage risk are then applied to that with DC power flow model to further calculate the corresponding optimal ED solutions. The total cost of ED solution is increased to $253590.58. The penalty of LOL in ED solutions is 53.81% higher than

that with overvoltage risk constraints. The reason is that unit commitment results with overvoltage risk constraints are more reliable against fluctuations of wind and solar generation, i. e., it could better accommodate volatility of renewables with reduced load shedding.

3) In this case, the voltage limit is used instead of overvoltage risk constraints. The amounts of LOL and spillage of wind and solar generation with overvoltage risk constraints and voltage limit are compared in Fig. 11. The penalty costs for LOL and spillage of wind and solar generation with voltage limit are $1878.00 and $165.95, respectively, higher than those with overvoltage risk constraints. With a stricter voltage constraint, more LOL and renewable energy spillage can be induced. By comparison, as long as the overvoltage risk is acceptable, the overvoltage is permitted for a short time to pursue the maximum system operation economics. Therefore, Case 4 with overvoltage risk constraints achieves a better tradeoff between the security and economics.
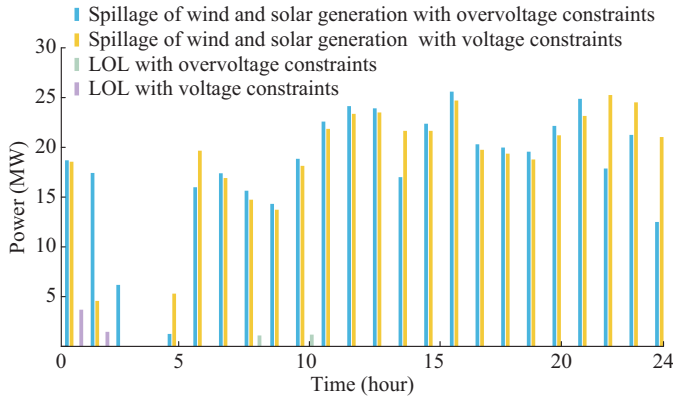

Fig. 11.   Spillage of wind and solar generation as well as LOL in Case 4.

B. IEEE 118-bus System

The modified IEEE 118-bus system includes 54 thermal units, 6 hydro units, 7 wind farms, 7 solar power stations, 186 branches, and 91 load buses. The total capacity of hydro units, wind energy, and solar energy are 725 MW, 1025 MW, and 1240 MW, respectively, which together account for about 30% of the total generation capacity. The peak load of 6000 MW occurs at hour 21.

The stochastic optimal model is solved with overvoltage risk constraints and voltage limit, respectively. The corresponding active power dispatches of thermal units are 55161.29 MWh and 57381.02 MWh, respectively. The total cost with overvoltage risk constraints is $1782513.61 about 3.97% lower than that with voltage limit.

Effectiveness of the improved PH is compared with the standard PH as shown in Fig. 12. It shows that because of binary variables in the second stage, the primal residue of basic PH keeps oscillating and the algorithm fails to converge after 70 iterations with the total cost of $1781041.70. Different settings of $x_{UB}=0.9, 0.8, 0.65$ and $x_{LB}=0.1, 0.2, 0.35$ are tested, together with the penalty factor $\varrho=60$, to illustrate the effectiveness of the improved PH algorithm in accelerating convergence performance while preserving high solution quality. With $x_{UB}=0.8$ and $x_{LB}=0.2$, the improved PH converges after 34 iterations; with $x_{UB}=0.65$ and $x_{LB}=$

0.35, the number of iterations is only 23, but the time corresponding to Steps 4 and 5 of the improved PH increases by 37.67%, and the total computing time is increased; with $x_{UB}=0.9$ and $x_{LB}=0.1$, the improved PH convergences after 70 iterations. The comparison shows that $x_{UB}=0.8$ and $x_{LB}=0.2$ is a proper setting for this test system, with which the improved PH outperforms the standard PH in terms of better convergence performance.
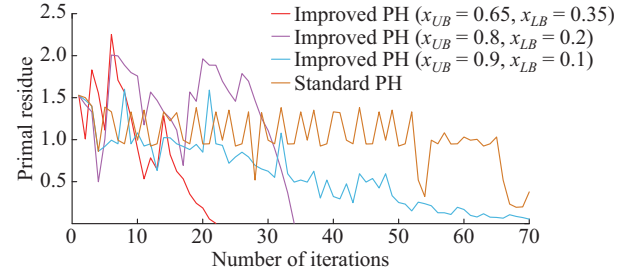

Fig. 12.   Convergence comparison.

To further understand the impact of scenarios on the performance of optimal solution, in terms of secure operation in handling out-of-sample scenarios [40], [41], 5 distinct sets of 10 scenarios are generated. The optimal unit commitment solution from one set is applied to all other 4 sets, re-optimizing the second-stage decisions, and calculating the total cost. The results are shown in Table VIII. It can be observed that the total cost fluctuation is within the range of 0.07%‐0.25%. The number of iterations for different sets ranges from 32 to 36. These results show that, for this system, the risk-constrained stochastic scheduling model with 10 scenarios can derive good suboptimal solutions and properly handle out-of-sample scenarios while mitigating the calculation burden.

TABLE VIII
COMPARISON OF DIFFERENT SCENARIO SET

Scenario set	Total cost ($)	Number of iterations	Error in cost (%)				
			Set 1	Set 2	Set 3	Set 4	Set 5
1	1782513.61	34		0.07	0.18	0.15	0.08
2	1783806.09	36	0.07		0.25	0.22	0.15
3	1779342.47	32	0.18	0.25		0.03	0.10
4	1779806.85	34	0.15	0.22	0.03		0.07
5	1781069.14	36	0.08	0.15	0.10	0.07	

VI. CONCLUSION

In this paper, a risk-constrained stochastic scheduling model is proposed to coordinate thermal, hydro, wind, and solar power considering uncertainties. The linearized AC power flow model enables that bus voltages are presented as variables to facilitate the overvoltage risk evaluation, which is further used to build probabilistic risk constraints in the proposed stochastic scheduling model. The proposed stochastic optimization model is solved by the progressive hedging framework, and a relax-round-polish heuristic process is developed to improve the convergence performance with high-quality solutions.

Simulation results show that: ① the proposed method enables the effective calculation on high-fidelity power system operation status (i.e., bus voltage and reactive power), which can effectively derive secure and economic system operation solutions; ② it increases the penetration level of wind and solar generation and helps reduce the total system operation cost, while potentially introducing high overvoltage risks against uncertainties; ③ compared with nodal voltage limits, overvoltage risk constraints can effectively balance the efficient utilization of renewable energy and secure operation of the system; ④ bundling renewable energy and traditional generation units can boost the utilization efficiency of renewable energy; ⑤ hydro units are valuable flexibility resources, but are limited by hydrological conditions, seasons, and other factors. In such situations, overvoltage risk constraints become more beneficial than nodal voltage limits as LOL induced by the limited accommodation capacity of hydro units can be reduced. In summary, the proposed risk-constrained stochastic scheduling model provides an appropriate way to coordinate the optimal operation of a mix of energy sources with uncertainties. Future work could include: ① evaluating potential impacts of different AC relaxation models on computational performance and solution quality of the day-ahead stochastic scheduling model; ② coordinating hierarchical operations of the system at different time resolutions, including day-ahead scheduling plan, hour/minute-ahead operation plan, and real-time control, to achieve overall operation security and economics.

APPENDIX A

A. Linearized AC Power Flow Calculation

The second-order Taylor series expansions of sine and cosine functions are used to approximate the nonlinear AC power flow model [23]. That is, as $\theta_{ij,t}^{\xi}$ is usually small, sine and cosine functions can be approximated via (A1).

$$\begin{cases} \sin\theta_{ij,t}^{\xi} \approx \theta_{ij,t}^{\xi} \\ \cos\theta_{ij,t}^{\xi} \approx 1 - \dfrac{\left(\theta_{ij,t}^{\xi}\right)^2}{2} \end{cases} \tag{A1}$$

Assuming voltage magnitude is close to 1.0 p.u., (A2) is further applied to decouple voltage and angle.

$$\begin{cases} V_{i,t}^{\xi}V_{j,t}^{\xi}\theta_{ij,t}^{\xi} \approx \theta_{ij,t}^{\xi} \\ V_{i,t}^{\xi}V_{j,t}^{\xi}\left(\theta_{ij,t}^{\xi}\right)^2 \approx \left(\theta_{ij,t}^{\xi}\right)^2 \end{cases} \tag{A2}$$

By substituting (A1) and (A2) into (12) and (13), (A3) and (A4) are obtained, where active power loss of line (i,j) $P_{ij,t}^{L,\xi}$ and reactive power loss of line (i,j) $Q_{ij,t}^{L,\xi}$ are given as (A5) and (A6), respectively.

$$P_{ij,t}^{\xi} = g_{ij}\frac{\left(V_{i,t}^{\xi}\right)^2 - \left(V_{j,t}^{\xi}\right)^2}{2} - b_{ij}\theta_{ij,t}^{\xi} + P_{ij,t}^{L,\xi} \tag{A3}$$

$$Q_{ij,t}^{\xi} = -b_{ij}\frac{\left(V_{i,t}^{\xi}\right)^2 - \left(V_{j,t}^{\xi}\right)^2}{2} - g_{ij}\theta_{ij,t}^{\xi} + Q_{ij,t}^{L,\xi} \tag{A4}$$

$$P_{ij,t}^{L,\xi} = \frac{1}{2}g_{ij}\left(\left(\theta_{ij,t}^{\xi}\right)^2 + \left(V_{ij,t}^{\xi}\right)^2\right) \tag{A5}$$

$$Q_{ij,t}^{L,\xi} = -\frac{1}{2}b_{ij}\left(\left(\theta_{ij,t}^{\xi}\right)^2 + \left(V_{ij,t}^{\xi}\right)^2\right) \tag{A6}$$

The loss-factor-based linearization method [23] is further used to facilitate the full linear reformulation of (A5) and (A6). That is, according to the base case operation condition of the system, losses can be linearized as in (A7) and (A8), where coefficients $\boldsymbol{P}_{LF,P,\theta}$, $\boldsymbol{P}_{LF,P,V^2}$, $\boldsymbol{P}_{LF,Q,\theta}$, and $\boldsymbol{P}_{LF,Q,V^2}$ are loss factors.

$$P_{ij,t}^{L,\xi} \approx \boldsymbol{P}_{LF,P,\theta}^{T}\boldsymbol{\theta}^{\xi} + \boldsymbol{P}_{LF,P,V^2}^{T}\left(\boldsymbol{V}^{\xi}\right)^2 + o_{P,ij} \tag{A7}$$

$$Q_{ij,t}^{L,\xi} \approx \boldsymbol{P}_{LF,Q,\theta}^{T}\boldsymbol{\theta}^{\xi} + \boldsymbol{P}_{LF,Q,V^2}^{T}\left(\boldsymbol{V}^{\xi}\right)^2 + o_{Q,ij} \tag{A8}$$

where $o_{P,ij}$ and $o_{Q,ij}$ are the active power offset and reactive power offset of line (i,j), respectively; and $\boldsymbol{\theta}^{\xi}$ and $\boldsymbol{V}^{\xi}$ are the voltage angle and amplitude vectors, respectively.

Finally, the linearized AC power flow model includes (A3), (A4), (A7), and (A8), which replace the original nonlinear constraints (11) and (12).

B. Piecewise Linearization of Branch Flow Limits

The piecewise linearization method described in [23] is used to facilitate the linear reformulation of the branch flow limit (13). Specifically, nonlinear equation in the form of $\left(P_{ij,t}^{\xi}\right)^2 + \left(Q_{ij,t}^{\xi}\right)^2 = \left(S_{ij}^{max}\right)^2$ can be transferred into n linear equations as shown in Fig. A1, where $P_{ij,t}^{\xi(A)}, Q_{ij,t}^{\xi(A)}, P_{ij,t}^{\xi(B)}, Q_{ij,t}^{\xi(B)}$ are the active and reactive power flows from bus i to bus j at time t and points A and B in scenario ξ, respectively. In Fig. A1, the line connecting points A and B on a circle with radius S_{ij}^{max} is used to approximate the segment of circle between A and B, which can be written as:

$$\left(\sin\left(\frac{360°k}{n}\right) - \sin\left(\frac{360°(k-1)}{n}\right)\right)P_{ij,t}^{\xi} - \left(\cos\frac{360°k}{n} - \cos\left(\frac{360°(k-1)}{n}\right)\right)Q_{ij,t}^{\xi} - S_{ij}^{max}\sin\left(\frac{360°}{n}\right) \leq 0 \quad k = 1, 2, ..., n \tag{A9}$$
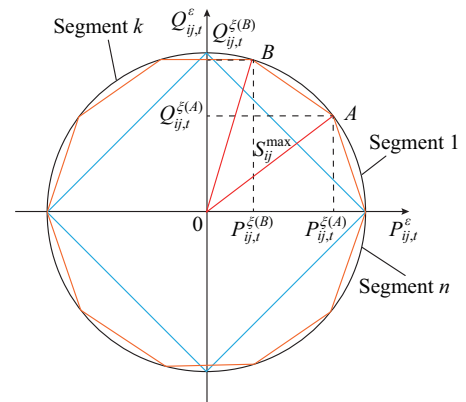

Fig. A1.   Linearization of quadratic branch flow limits.

C. Piecewise Linearization of Water-to-power Conversion Function

Equation (27) expresses the nonlinear water-to-power conversion curve with two variables, which can be converted into a piecewise linear representation (A10)-(A15) via the heuristic method [42], [43], and is further divided into two triangles, i.e., upper left and lower right.

$$\sum_{x=}^{N_x}\sum_{y=1}^{N_y}\lambda_{x,y}=1 \quad \lambda_{x,y}\geq 0 \tag{A10}$$

$$\begin{cases} R=\sum_{x=}^{N_x}\sum_{y=1}^{N_y}R_x\lambda_{x,y} \\ \\ L=\sum_{x=}^{N_x}\sum_{y=1}^{N_y}L_y\lambda_{x,y} \end{cases} \tag{A11}$$

$$\sum_{x=1}^{N_x}\sum_{y=1}^{N_y}\left(u_{x,y}+v_{x,y}\right)=1 \quad u_{x,y},v_{x,y}\in\{0,1\} \tag{A12}$$

$$\lambda_{x,y}\leq u_{x,y-1}+u_{x,y}+u_{x,y+1}+v_{x-1,y}+v_{x,y}+v_{x+1,y} \tag{A13}$$

$$P_h=\sum_{x=}^{N_x}\sum_{y=1}^{N_y}\lambda_{x,y}p_{h,x,y} \tag{A14}$$

$$p_{h,x,y}=\eta_h L_y\left(h_h^0+\alpha_h R_x\right) \tag{A15}$$

where N_x, N_y, and $\lambda_{x,y}$ are the number of vertical piecewise segment, number of horizontal piecewise segment and location of triangles, respectively; R_x and L_y are the reservoir volume of horizontal piecewise segment and the water discharge of vertical piecewise segment, respectively; $u_{x,y}$ and $v_{x,y}$ are the indices to represent the locations in the two triangles, respectively; P_h is the active power of hydro unit i_h; and $p_{h,x,y}$ is the head-dependent water-to-power conversion function.

Thus, the head-dependent water-to-power conversion func-

tion is given.

D. Data of Generators

TABLE AI
THERMAL GENERATOR DATA

Unit	Active power (MW)		Reactive power (MW)		Up/down time (hour)	Ramp (MW/h)
	Lower	Upper	Lower	Upper		
G1	30	80	−20	150.0	8	40
G2	30	80	−20	60.0	4	30
G3	20	50	−15	62.5	3	40
G4	20	55	−15	48.7	3	20
G5	20	30	−10	40.0	3	20
G6	25	40	−15	44.7	3	20

TABLE AII
FUEL DATA

Unit	Coefficient a (MBtu)	Coefficient b (MBtu/MWh)	Coefficient c (MBtu/MW²h)	Start-up fuel (MBtu)	Fuel price ($/MBtu)
G1	0.0024	12.33	28.00	1500	2.5
G2	0.0459	15.47	74.33	100	2.5
G3	0.0128	17.82	10.15	50	2.5
G4	0.0080	14.50	42.00	50	2.5
G5	0.0044	13.29	39.00	50	2.5
G6	0.0459	15.47	74.33	100	2.5

TABLE AIII
HYDRO GENERATOR DATA

Unit	Efficiency	h_0	α	Discharge (m³)		On/off time (hour)	Volume (m³)		Ramp (MW/hour)	Generation (MW)		Natural inflow (m³)
				Maximum	Minimum		Maximun	Mimimum		Lower	Upper	
H1	5.636	0.071	0.0071	6×10⁵	0	1	1.4×10⁶	4×10⁵	60	7	115	2×10⁵
H2	8.091	0.791	0.0012	8×10⁵	0	1	1.6×10⁶	6×10⁵	80	7	120	3×10⁵

REFERENCES

[1] H. Zhang, J. Zhou, Y. Zhang et al., "Culture belief based multi-objective hybrid differential evolutionary algorithm in short term hydrothermal scheduling," *Energy Conversion and Management*, vol. 65, pp. 173-184, Jan. 2013.

[2] Z. Qin, W. Li, and X. Xiong, "Generation system reliability evaluation incorporating correlations of wind speeds with different distributions," *IEEE Transactions on Power Systems*, vol. 28, no. 1, pp. 551-558, Feb. 2013.

[3] C. Luo, H. Banakar, B. Shen et al., "Strategies to smooth wind power fluctuations of wind turbine generator," *IEEE Transactions on Energy Conversion*, vol. 22, no. 2, pp. 341-349, Jun. 2007.

[4] A. Rusin and A. Wojaczek, "Trends of changes in the power generation system structure and their impact on the system reliability," *Energy*, vol. 92, pp. 128-134, Dec. 2015.

[5] R. Hemmati, H. Saboori, and S. Saboori, "Stochastic risk-averse coordinated scheduling of grid integrated energy storage units in transmission constrained wind-thermal systems within a conditional value-at-risk framework," *Energy*, vol. 113, pp. 762-775, Oct. 2016.

[6] Y. Wang, L. Huang, M. Shahidehpour et al., "Resilience-constrained hourly unit commitment in electricity grids," *IEEE Transactions on Power Systems*, vol. 33, no. 5, pp. 5604-5614, Sept. 2018.

[7] M. A. Tajeddini, A. Rahimi-Kian, and A. Soroudi, "Risk averse optimal operation of a virtual power plant using two stage stochastic programming," *Energy*, vol. 73, pp. 958-967, Aug. 2014.

[8] P. Kundur, N. Balu, and M. Lauby, *Power System Stability and Control*, New York: McGraw-Hill, 1994.

[9] J. Aghaei, A. Nikoobakht, P. Siano et al., "Exploring the reliability effects on the short term AC security-constrained unit commitment: a stochastic evaluation," *Energy*, vol. 114, pp. 1016-1032, Nov. 2016.

[10] A. Rabiee, S. Nikkhah, and A. Soroudi, "Information gap decision theory to deal with long-term wind energy planning considering voltage stability," *Energy*, vol. 147, pp. 451-463, Mar. 2018.

[11] A. Rabiee, A. Soroudi, B. Mohammadi-Ivatloo et al., "Corrective voltage control scheme considering demand response and stochastic wind power," *IEEE Transactions on Power Systems*, vol. 29, no. 6, pp. 2965-2973, Nov. 2014.

[12] N. Amjady, J. Aghaei, and H. A. Shayanfar, "Stochastic multiobjective market clearing of joint energy and reserves auctions ensuring power system security," *IEEE Transactions on Power Systems*, vol. 24, no. 4, pp. 1841-1854, Nov. 2009.

[13] T. T. Nguyen, "A high performance social spider optimization algorithm for optimal power flow solution with single objective optimization," *Energy*, vol. 171, pp. 218-240, Mar. 2019.

[14] A. J. Wood and B. F. Wollenberg, *Power Generation, Operation and Control*, New York: Wiley, 1996.

[15] T. N. Dos Santos and A. L. Diniz, "A dynamic piecewise linear model for DC transmission losses in optimal scheduling problems," *IEEE Transactions on Power Systems*, vol. 26, no. 2, pp. 508-519, May 2011.

[16] H. Zhong, Q. Xia, Y. Wang et al., "Dynamic economic dispatch con-

sidering transmission losses using quadratically constrained quadratic program method," *IEEE Transactions on Power Systems*, vol. 28, no. 3, pp. 2232-2241, Aug. 2013.

[17] A. Castillo, P. Lipka, J. P. Watson *et al.*, "A successive linear programming approach to solving the IV-ACOPF," *IEEE Transactions on Power Systems*, vol. 31, no. 4, pp. 2752-2763, Jul. 2016.

[18] Z. Yang, H. Zhong, Q. Xia *et al.*, "A novel network model for optimal power flow with reactive power and network losses," *Electric Power Systems Research*, vol. 144, pp. 63-71, Mar. 2017.

[19] C. Z. Karatekin and C. Uçak, "Sensitivity analysis based on transmission line susceptances for congestion management," *Electric Power Systems Research*, vol. 78, no. 9, pp. 1485-1493, Sept. 2008.

[20] B. Leonardi and V. Ajjarapu, "Investigation of various generator reactive power reserve (GRPR) definitions for online voltage stability/security assessment," in *Proceedings of Power and Energy Society General Meeting － Conversion and Delivery of Electrical Energy in the 21st Century*, Pittsburgh, USA, Jul. 2008, pp. 1-7.

[21] M. Esmaili, H. A. Shayanfar, and N. Amjady, "Multi-objective congestion management incorporating voltage and transient stabilities," *Energy*, vol. 34, no. 9, pp. 1401-1412, Sept. 2009.

[22] J. D. McCalley, A. A. Fouad, V. Vittal *et al.*, "A risk-based security index for determining operating limits in stability-limited electric power systems," *IEEE Transactions on Power Systems*, vol. 12, no. 3, pp. 1210-1219, Aug. 1997.

[23] Z. Yang, H. Zhong, A. Bose *et al.*, "A linearized OPF model with reactive power and voltage magnitude: a pathway to improve the MW-only DC OPF," *IEEE Transactions on Power Systems*, vol. 33, no. 2, pp. 1734-1745, Mar. 2018.

[24] M. Ni, J. D. McCalley, V. Vittal *et al.*, "Online risk-based security assessment," *IEEE Transactions on Power Systems*, vol. 18, no. 1, pp. 258-265, Feb. 2003.

[25] R. Preece and J. V. Milanović, "Risk-based small-disturbance security assessment of power systems," *IEEE Transactions on Power Delivery*, vol. 30, no. 2, pp. 590-598, Apr. 2015.

[26] J. P. Watson and D. L. Woodruff, "Progressive hedging innovations for a class of stochastic mixed-integer resource allocation problems," *Computational Management Science*, vol. 8, no. 4, pp. 355-370, Nov. 2011.

[27] B. W. Silverman, *Density Estimation for Statistics and Data Analysis*, New York: Chapman & Hall, 1986.

[28] L. Wu, M. Shahidehpour, and T. Li, "Stochastic security-constrained unit commitment," *IEEE Transactions on Power Systems*, vol. 22, no. 2, pp. 800-811, May 2007.

[29] Y. Yin, T. Q. Liu, and C. He. (2019, Nov.). Day-ahead stochastic coordinated scheduling for thermal-hydro-wind-photovoltaic systems. [Online]. Available: https://www. sciencedirect. com/science/article/abs/pii/S0360544219316287

[30] S. Kamalinia, L. Wu, and M. Shahidehpour, "Stochastic midterm coordination of hydro and natural gas flexibilities for wind energy integration," *IEEE Transactions on Sustainable Energy*, vol. 5, no. 4, pp. 1070-1079, Oct. 2014.

[31] X. Wang, J. Chang, X. Meng *et al.*, "Short-term hydro-thermal-wind-photovoltaic complementary operation of interconnected power systems," *Applied Energy*, vol. 229, pp. 945-962, Nov. 2018.

[32] C. He, L. Wu, T. Liu *et al.*, "Robust co-optimization scheduling of electricity and natural gas systems via ADMM," *IEEE Transactions on Sustainable Energy*, vol. 8, no. 2, pp. 658-670, Apr. 2017.

[33] L. Wu, M. Shahidehpour, and T. Li, "GENCO's risk-based maintenance outage scheduling," *IEEE Transactions on Power Systems*, vol. 23, no. 1, pp. 127-136, Feb. 2008.

[34] A. Moreira, A. Street, and J. M. Arroyo, "An adjustable robust optimization approach for contingency-constrained transmission expansion planning," *IEEE Transactions on Power Systems*, vol. 30, no. 4, pp. 2013-2022, Jul. 2015.

[35] C. Sahin, M. Shahidehpour, and I. Erkmen, "Allocation of hourly reserve versus demand response for security-constrained scheduling of stochastic wind energy," *IEEE Transactions on Sustainable Energy*, vol. 4, no. 1, pp. 219-228, Jan. 2013.

[36] M. Pai, *Computer Methods in Power System Analysis*, New York: McGraw-Hill Book Co., 1996.

[37] Elia. (2019, Jan.). Belgium's electricity transmission system operator. [Online]. Available: http://www. elia. be/en/grid-data/power-generation/wind-power

[38] M. Marsadek, A. Mohamed, and Z. Norpiah. "Assessment and classification of line overload risk in power systems considering different types of severity functions," *WSEAS Transactions on Power Systems*, vol. 5, no. 3, pp. 182-191, 2010.

[39] N. Aminudin, N. M. Ramli, M. Marsadek *et al.*, "Classification of risk of voltage collapse using risk matrix," in *Proceedings of 2016 IEEE International Conference on Power System Technology (POWERCON)*, Wollongong, Australia, Sept. 2016, pp. 1-5.

[40] T. Ding, Q. Yang, X. Liu *et al.*, "Duality-free decomposition based data-driven stochastic security-constrained unit commitment," *IEEE Transactions on Sustainable Energy*, vol. 10, no. 1, pp. 82-93, Jan. 2019.

[41] L. Wu, M. Shahidehpour, and Z. Y. Li, "Comparison of scenario-based and interval optimization approaches to stochastic SCUC," *IEEE Transactions on Power Systems*, vol. 27, no. 2, pp. 913-921, May 2012.

[42] D. A. Babayev, "Piece-wise linear approximation of functions of two variables," *Journal of Heuristics*, vol. 2, no. 4, pp. 313-320, Mar. 1997.

[43] C. Hamon, M. Perninge, and L. Söder, "A stochastic optimal power flow problem with stability constraints － part I: approximating the stability boundary," *IEEE Transactions on Power Systems*, vol. 28, no. 2, pp. 1839-1848, May 2013.

Yue Yin received her B.S. degree in electrical engineering from Jimei University, Xiamen, China, in 2006, and M.S. degree in electrical engineering from Sichuan University, Chengdu, China, in 2010, respectively. Currently, she is a Lecturer in College of Electrical Engineering at Sichuan University, and is presently Ph.D. student in the College of Electrical Engineering, Sichuan University. Her main research interests include power system stability, HVDC, optimal generation dispatch, and dynamic security analysis.

Tianqi Liu received the B. S. and M. S. degrees in electrical engineering from Sichuan University, Chengdu, China, in 1982 and 1986, respectively, and the Ph.D. degree in electrical engineering from Chongqing University, Chongqing, China, in 1996. Currently, she is a Professor in School of Electrical Engineering at Sichuan University. Her main research interests include power system analysis and stability control, HVDC, optimal operation, dynamic security analysis, dynamic state estimation and load forecasting.

Lei Wu received the B.S. degree in electrical engineering and the M.S. degree in systems engineering from Xi'an Jiaotong University, Xi'an, China, in 2001 and 2004, respectively, and the Ph.D. degree in electrical engineering from Illinois Institute of Technology (IIT), Chicago, USA, in 2008. From 2008 to 2010, he was a Senior Research Associate with the Robert W. Galvin Center for electricity innovation. He worked as summer visiting faculty at New York Independent System Operator (NYISO) in 2012. Currently, he is a Professor with the Electrical and Computer Engineering Department, Stevens Institute of Technology, Hoboken, USA. His research interests include power system operation and planning, energy economics, and community resilience microgrid.

Chuan He received the B.S, M.S and Ph.D. degrees from Sichuan University, Chengdu, China. Currently, he is a Lecturer in College of Electrical Engineering at Sichuan University. His research interests include robust optimization on power system operation and planning with renewable energy.

Yikui Liu received the B.S. degree from Nanjing Institute of Technology, Nanjing, China, in 2012, the M.S. degree from Sichuan University, Chengdu, China, in 2015, and the Ph.D. degree from Stevens Institute of Technology, Hoboken, USA, in 2020, respectively, all in electrical engineering. Currently, he is an Engineer of Siemens, Minneapolis, USA. His main research interests include power system analysis and stability control, HVDC, dynamic security analysis, dynamic state estimation and load forecasting.